Materials and Design 142 (2018) 247–258

Contents lists available at ScienceDirect

Materials and Design

journal homepage: www.elsevier.com/locate/matdes

Exploiting negative Poisson's ratio to design 3D-printed composites with enhanced mechanical properties

Tiantian Li [a], Yanyu Chen [b], Xiaoyi Hu [a], Yangbo Li [a,c], Lifeng Wang [a,*]

[a] Department of Mechanical Engineering, Stony Brook University, Stony Brook, NY 11794, USA
[b] Transportation and Hydrogen Systems Center, National Renewable Energy Laboratory, Golden, CO 80401, USA
[c] College of Hydraulic & Environmental Engineering, China Three Gorges University, Yichang, Hubei 443002, China

HIGHLIGHTS

- A new class of two-component composites with auxetic structures are designed and fabricated using 3D printing technique.
- The auxetic lattice reinforced composites exhibit enhanced stiffness and energy absorption under uniaxial compression.
- The degree of auxetic behavior can be used to tune the stiffness and energy absorption of the composites.
- The re-entrant honeycomb reinforced composite exhibits a nearly linear scaling relation.

GRAPHICAL ABSTRACT

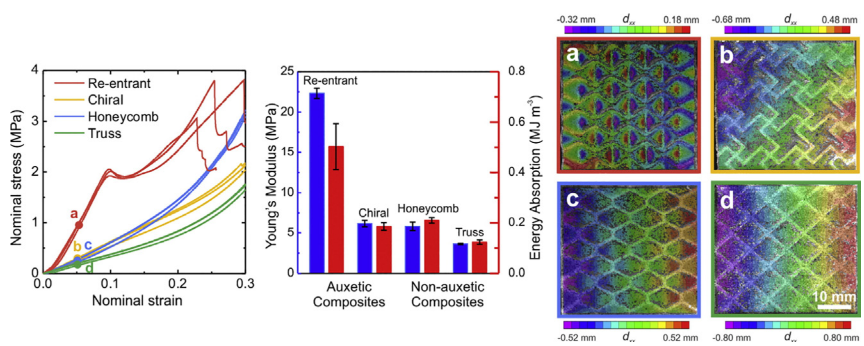

ARTICLE INFO

Article history:
Received 15 November 2017
Received in revised form 3 January 2018
Accepted 18 January 2018
Available online 3 February 2018

Keywords:
Auxetics
3D printing
Stiffness
Energy absorption
Composites
Lattice materials

ABSTRACT

Auxetic materials exhibiting a negative Poisson's ratio are shown to have better indentation resistance, impact shielding capability, and enhanced toughness. Here, we report a class of high-performance composites in which auxetic lattice structures are used as the reinforcements and the nearly incompressible soft material is employed as the matrix. This coupled geometry and material design concept is enabled by the state-of-the-art additive manufacturing technique. Guided by experimental tests and finite element analyses, we systematically study the compressive behavior of the 3D printed auxetics reinforced composites and achieve a significant enhancement of their stiffness and energy absorption. This improved mechanical performance is due to the negative Poisson's ratio effect of the auxetic reinforcements, which makes the matrix in a state of biaxial compression and hence provides additional support. This mechanism is further supported by the investigation of the effect of auxetic degree on the stiffness and energy absorption capability. The findings reported here pave the way for developing a new class of auxetic composites that significantly expand their design space and possible applications through a combination of rational design and 3D printing.

1. Introduction

Materials exhibiting a negative Poisson's ratio, also called auxetic materials [1], are a new type of mechanical metamaterials which will contract (expand) transversally when they are axially compressed (stretched). Since the 1980s, auxetic behavior has been reported in many two-dimensional (2D) and three-dimensional (3D) structures of natural systems, including cubic metals [2], zeolites [3,4], natural

* Corresponding author.
E-mail address: lifeng.wang@stonybrook.edu (L. Wang).

https://doi.org/10.1016/j.matdes.2018.01.034
0264-1275/

layered ceramics [5], silicon dioxides [6], single-layer graphene [7,8], and 2D protein crystals [9]. Since the auxetic behavior potentially equips materials with improved properties, including shear modulus [10], indentation resistance [11], fracture toughness [12–14], and energy absorption ability [1,15–19], there are significant interests in the development of negative Poisson's ratio materials because of their potential applications, such as textile [20–23], automotive [24], military [25,26], biomedical [27,28], and aerospace engineering [29]. Research in this area has begun from the computational works of Wojciechowski [30] as well as the development of 3D polymeric foams with isotropic auxetic behavior by Lakes [10]. Subsequently, several geometries and mechanisms have been proposed to achieve a negative Poisson's ratio and a significant body of man-made auxetic materials and structures has been fabricated and synthesized from the macroscopic down to molecular levels. Among them, there are in planar foams [31], honeycombs with inverted cells [32–34], 2D and 3D chiral lattices [35–40], rigid rotating hexamers or squares [41–44], origami/kirigami based metamaterials [45–50] and hierarchical metamaterials with fractal cuts [51–53]. Recently, theoretical models indicate the possibility to achieve auxeticity in some colloidal crystals [54]. A detailed analysis of the deformation mechanisms of 2D and 3D auxetics can be found in Ref [55]. Due to the bending or rotation deformation nature of the ligaments/elements in these auxetic materials, however, they usually have relatively low stiffness, limiting their applications where lightweight, high stiffness, strength, and energy absorption are simultaneously desired.

Composite materials with rationally designed structures and compositions could overcome this limitation. In a two-phase composite, each constituent phase can contributes its own properties in a quite independent manner to the overall performance of the composites synergistically. For example, composite materials where auxetic lattice structures are used as the reinforcements and the nearly incompressible soft material is employed as a matrix have great potential in achieving a design to combine these prominent mechanical properties. Conceptually, by harnessing the negative Poisson's ratio effect of the auxetic reinforcement, the soft matrix will be in a state of biaxial or triaxial compression, resulting in a synergistic improvement in the mechanical response. Indeed, composites materials with auxetic reinforcements have been designed and fabricated in the past few decades. The auxetic fibers embedded in the composite as the reinforcement would expand when stretched and prevent the occurring of fiber pullout, therefore, the load required to cause structural failure will significantly increase [56–58]. In addition, composites using 3D auxetic textile structures as the reinforcement have been fabricated and exhibited strong auxetic behavior [59]; however, relatively poor mechanical properties are observed as compared with non-auxetic composites [60]. Composites with elliptic inclusions exhibit auxetic effect with relative lower Young's modulus compared with the non-auxetic composites as evidenced by the finite element analysis [61]. It should be pointed out that these undesired mechanical properties of composite materials with auxetic reinforcements are partially due to the limitation of conventional manufacturing techniques. In this regard, additive manufacturing techniques have shown unparalleled advantages, as they enable us to fabricate complex topologies with fine features quickly, cheaply, and at a large scale, and offer a multitude of materials with varying mechanical properties [62,63]. For example, auxetic structures fabricated using selective laser sintering and filled with strain rate sensitive material exhibit slightly increased energy absorption ability during impact tests [64]. Despite considerable efforts have been devoted to designing and synthesizing composites with auxetic reinforcements, the quantitative understanding of the interplay between the auxetic behavior and the other mechanical properties such as stiffness, strength, and toughness is still elusive. For example, systematic studies on mechanical properties of the composites with auxetic reinforcements in comparison with non-auxetic reinforcements have not been largely explored [15,57,65]. Furthermore, the effect of negative Poisson's ratio on the mechanical properties such as stiffness, strength, and energy absorption of the auxetic composites is still not clear.

In this work, we design a group of composite materials consisting of two types of auxetic reinforcements and a nearly incompressible soft elastomer as the filled matrix. The coupled geometry and material design concept is realized by an advanced 3D printing technique, which enables the fabrication of bimaterial composites with various geometries and material selections. Uniaxial compression tests are conducted to investigate the mechanical properties of these composite materials with auxetic reinforcements. Finite element simulations are performed to provide additional insights into the underlying mechanisms responsible for the observed unusual mechanical performance. Moreover, parametric analyses are conducted to quantitatively understand the effects of Poisson's ratio and volume fraction of the auxetic reinforcements on the mechanical properties of the auxetic reinforced composites.

2. Materials and methods

2.1. Design of auxetic lattice reinforced composites

The model system of the auxetic reinforced composites studied here is based on microstructures which combine the lattice structures and their inverse domains. Here two types of auxetic lattice structures are considered including a re-entrant honeycomb and a chiral truss, as shown in Fig. 1(a). For the purpose of comparisons, two types of regular lattice structures exhibiting a non-negative Poisson's ratio are also designed (Fig. 1(a)). By filling the inverse domains of each lattice structure with another material as the matrix, we can design the lattice structure reinforced composites. The symmetry and volume distribution in these structures can be precisely controlled by tailoring the thickness of ligaments in each lattice structure. Fig. 1(b) displays the proposed re-entrant honeycomb reinforced composites, chiral truss reinforced composites, regular honeycomb reinforced composites, and truss reinforced composites, where the volume fractions of the reinforcing phase are all set to 20%. In our designs, the phase of lattice structures is set as the reinforced domain, which is fabricated with a glassy polymer (VeroWhite), and the inversed phase is set as the matrix domain, which is fabricated with a rubber-like material (TangoPlus).

2.2. Sample fabrication

The specimens are fabricated using an Objet Connex260 multi-material 3D printer (Stratasys, Ltd), which allows simultaneous printing of two different materials. The specimens for compression tests consist of 4×4 unit cells, resulting in prototype dimensions of 40 mm $\times$ 40 mm, which are shown in Fig. 1(c). Focusing on the 2D in-plane mechanical behavior of these structures, we, therefore, design the thickness of the specimens as 20 mm to avoid the out-of-plane deformation. The minimum geometric size of the lattice reinforcement in the composites is around 200 μm, which is at least one order of magnitude greater than the minimum resolution (16 μm) provided by the 3D printer. Considering the anisotropic nature of the 3D printing, all the specimens are printed along the same orientation to avoid the influence of the layer orientation on the mechanical properties of the material. The as-fabricated specimens are kept at room temperature for 7 days to allow for the saturation of the curing.

2.3. Mechanical testing

To capture the mechanical response of the 3D printed constituent materials (VeroWhite and TangoPlus), the uniaxial compression tests of cylinder samples are performed based on ASTM D695 standard. The uniaxial compression tests for cylinder samples and the cubic composite samples are performed using a MTS mechanical tester (C43) with a 10 kN load cell. All the experiments are conducted in a quasi-static regime with a constant strain rate of 0.001 s^{-1}. The load-displacement curves

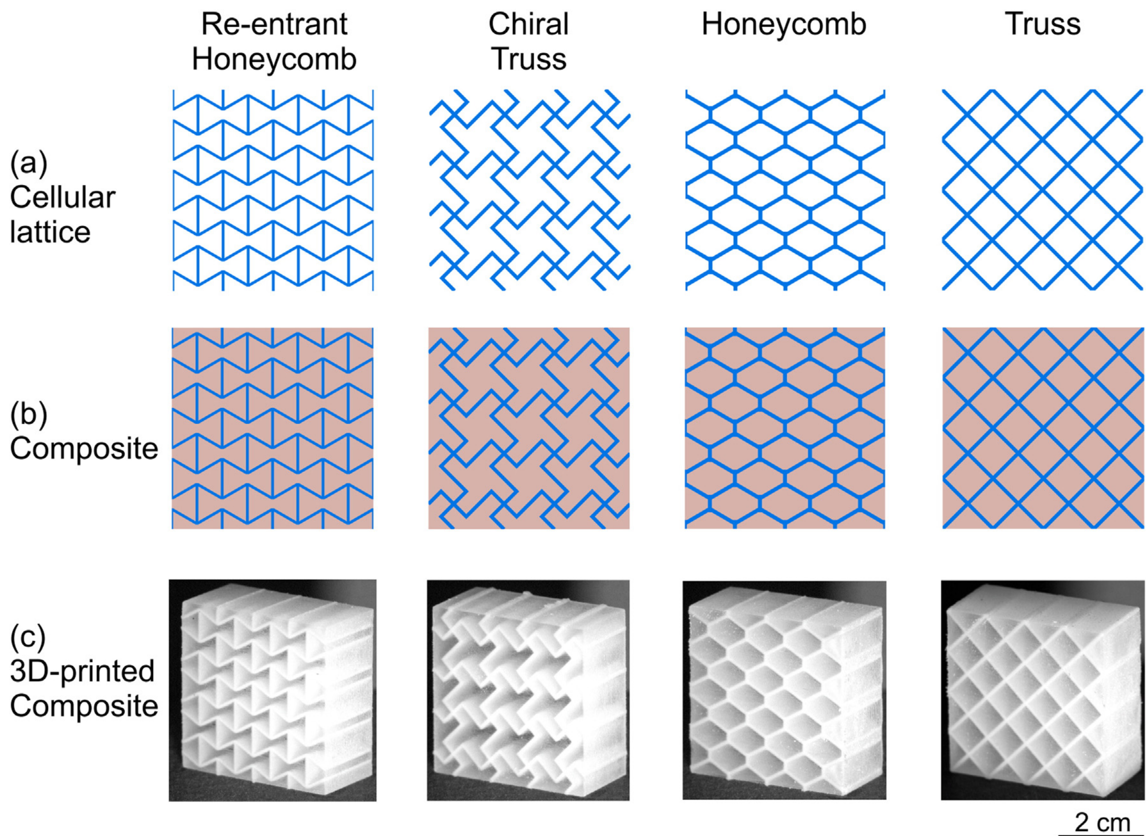

Fig. 1. Schematics of (a) lattice structures, (b) lattice reinforced composite structures and (c) 3D-printed lattice reinforced composite specimens consisting of 4 × 4 unit cells with re-entrant honeycomb, chiral truss, honeycomb, and truss structures.

measured from the uniaxial compression tests are then transferred into nominal stress-strain behaviors based on the measured dimensions of the specimens. Young's modulus is calculated from the initial linear region of the nominal stress-strain curves. The energy absorption is computed as the work under the nominal stress-strain curve before 25% uniaxial compressive strain for each composite sample. Images of the specimens at various loading conditions are taken at a rate of 1 FPS (Vic Snap, Correlated Solution). The deformation and displacement contours of the samples are tracked by using DIC (Vic-2D, Correlated Solution). The image processing software (ImageJ 1.49 q) is used to determine the displacement of the center area of the specimens in order to calculate the Poisson's ratio at each level of applied compression.

2.4. Finite element analysis

The numerical simulations related to the mechanical response of the lattice reinforced composites under uniaxial compression are conducted using the commercial FE package ABAQUS/Standard (Simulia, Providence, RI). Models with 4 × 4 unit cells are used in all of the simulations. All models are generated by plane strain elements CPE4R and meshed after a convergence test. In addition, geometric and material nonlinearities are taken into consideration to enable the large deformation of the structure. Due to the layer by layer manufacture process of 3D printing, the mechanical properties of the printed samples strongly depend on the printing directions [66]. While in our numerical simulations, an isotropic material model is adopted. The constituent phases are taken to be a glassy polymer and an elastomer material. The stress-strain behavior of the glassy polymer is captured using an elastic-viscoplastic model which is exported from the true stress-strain relation of VeroWhite as shown in Fig. 2. The elastomeric stress-strain behavior of TangoPlus is modeled as a hyperelastic material based on the Arruda-Boyce hyperelastic model [67] with an initial shear modulus of 0.213 MPa and locking stretch of 1.90. To simulate the experimental conditions in the numerical analysis, a uniaxial displacement loading is applied on the top surface, while the bottom is fixed along the vertical direction.

3. Results and discussion

3D printed constitutive materials are first mechanically tested under uniaxial compression by following the ASTM D695 standard. Fig. 2 shows the compressive stress-strain responses of the two constitutive materials and the mechanical properties extracted from these stress-strain curves are presented in Table 1. For the 3D printing material VeroWhite, the stress-strain behavior exhibits initial linear elasticity, yielding, post-yield, strain softening, and subsequent strain hardening at larger strains (see Fig. 2(a)). While for 3D printing material TangoPlus, the stress-strain curve is J-shape indicating a hyperelastic behavior. These measured mechanical responses and extracted data will be implemented in the commercial finite element software.

3.1. Mechanical response of auxetic lattice reinforced composites

We first examine the compressive behavior of the auxetic lattice reinforced composites from an experimental standpoint. Four types of architected lattice reinforced composites with re-entrant honeycomb, chiral lattice, regular honeycomb, truss lattice topology are fabricated using 3D printing (Fig. 3(a)). Here, we use the same volume fraction of reinforcement phase of 20%. The stress-strain curves show good repeatability for each composite as can be seen in Fig. 3(b). The re-entrant honeycomb reinforced composites demonstrate clear superiority over the other three composites. A sudden drop in the stress-strain response of the re-entrant honeycomb reinforced composites is observed after the stress reaches its maximum. This is because of the

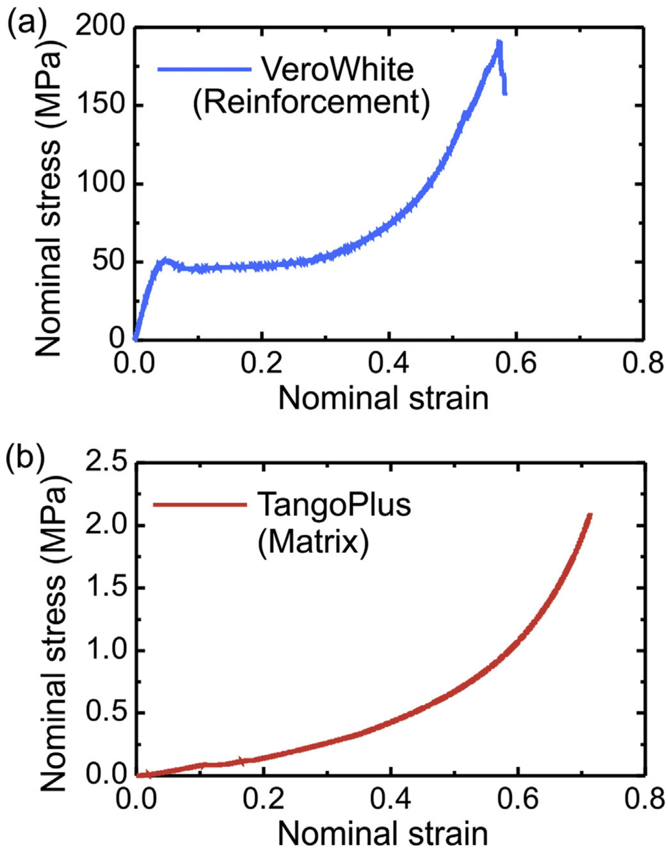

Fig. 2. The stress-strain response of the (a) VeroWhite (reinforcement phase) and (b) TangoPlus (matrix phase) materials used in this study.

instability of the re-entrant honeycomb structures during compressive deformation which will locally maximize the stress, resulting in a catastrophic failure. While the curves of the chiral lattice, regular honeycomb, and truss honeycomb reinforced composites exhibit smooth curved transition up to a strain of 0.3, which is due to the stability of the structures. Fig. 3(c) quantitatively shows that the Young's modulus of the re-entrant honeycomb reinforced composites is four times larger than that of the chiral truss and regular honeycomb reinforced composites, and five times larger than that of the truss reinforced composites. Moreover, the energy absorption at a strain of 25% of the re-entrant honeycomb reinforced composites is three times larger than that of other three types of composites. Because the re-entrant honeycomb lattice [68] and the chiral lattice [36] are two typical auxetic structures with negative Poisson's ratio effect (see in Fig. 4(e)), these results clearly show the advantage of employing auxetic lattice geometries especially re-entrant honeycomb structures in enhancing the mechanical properties of lattice reinforced composites.

Fig. 4 shows a series of images that exhibit the deformation behavior of these four lattice reinforced composites at different strain levels. It is clear that at a small compressive strain (<0.05), the re-entrant honeycomb reinforced composites exhibit a lateral shrinkage in average, which indicates that the auxetic lattice reinforced composite still has auxetic behavior at small deformation, as shown in Fig. 4(a). However, the instability of re-entrant honeycomb reinforced composite can be observed starting from the strain of 0.1, resulting in a peak stress in the stress-strain curve as seen in Fig. 3(b). Moreover, the instability of the structures under continuous compressive loading causes a local stress concentration, leading to the failure of the re-entrant honeycomb reinforced composite at a strain of around 0.3. Although the chiral lattice is also an auxetic structure, the chiral lattice reinforced composites do not exhibit obvious auxetic behavior at small deformation, as shown in Fig. 4(b). This is because the matrix elastomer as the inverse phase inhibits the rotation of the chiral reinforcement phase, resulting in a reduced lateral shrinkage. In contrast to the auxetic lattice reinforced composites, both the regular honeycomb and the truss reinforced composites exhibit a clear lateral expansion during the deformation in Fig. 4(c)–(d). Fig. 4(e) shows the experimental and numerical study of the Poisson's ratios for all four lattice reinforced composites and their corresponding cellular counterparts under uniaxial compression tests. To quantify the deformation taking place in the composites during the experiments, we calculate the deformation change by identifying four points in the center avoiding the deformation near the four edges of the specimen under the influence of boundary conditions, see in Fig. 4(f). Here, the rectangular frames represent the original edges of the specimens before the compressive deformation. One can notice the lateral shrinkage of the re-entrant honeycomb reinforced composite, slightly lateral shrinkage combined with the rotation of the chiral lattice reinforced composite and the lateral expansion of the honeycomb and truss reinforced composites at a macroscopic compressive strain of 0.05. Experimental and numerical results related to the Poisson's ratios are in excellent agreement for the four types of composites. Note that, for non-auxetic structures (truss and regular honeycomb), the Poisson's ratios of the composites and the corresponding cellular counterparts are almost identical, indicating no change in terms of deformation mechanism. However, for the chiral lattice, the Poisson's ratios of the composite are negative and much larger than that of the cellular counterpart. This is because the matrix phase obstructs the rotation of the chiral lattice, which decreases the auxetic behavior of structures. Moreover, for re-entrant honeycomb, the Poisson's ratio of the composite is slightly larger than that of the cellular counterpart, indicating that the matrix phase has minor effects on the shrinkage of re-entrant honeycomb lattice. Therefore, the re-entrant honeycomb reinforced composites also have as strong auxetic behavior as the re-entrant honeycomb cellular counterpart. This auxetic behavior of the composites contributes the enhancement of mechanical properties of the auxetic lattice reinforced composites.

To further understand the compressive behavior of these lattice reinforced composites and explain the superior mechanical properties of re-entrant honeycomb reinforced composites, we use Digital Image Correlation (DIC) (VIC-2D, Correlated Solutions) to analyze the experimental displacement contours. The images in Fig. 5 exhibit the horizontal displacement contours of four lattice reinforced composites at a vertical compressive strain of 0.05. We notice that the re-entrant honeycomb reinforcement phase exhibit shrinkage in the horizontal direction which increases the load transfer between the glassy polymer and the elastomer in Fig. 5(a). The chiral lattice reinforced composite has the asymmetry displacement contours on the surface, as shown in Fig. 5(b), due to the rotation mechanism when deformed. Compared with auxetic reinforced composites, the regular honeycomb, and the truss reinforced composite exhibit clear homogeneous horizontal expansion both in reinforcement phase and matrix phase, as shown in Fig. 5(c)–(d). It is clear that in non-auxetic reinforced composites the elastomer

Table 1
Mechanical properties of the 3D-printed constitutive materials.

Material	Young's modulus (MPa)	Compressive yield strength (MPa)	Ultimate compressive strength (MPa)	Toughness (J/m^3)	Energy absorption (strain = 0.25) (J/m^3)
VeroWhite	1513	50.5	187.5	42.3	11.0
TangoPlus	0.77	–	~2.1	0.38	0.02

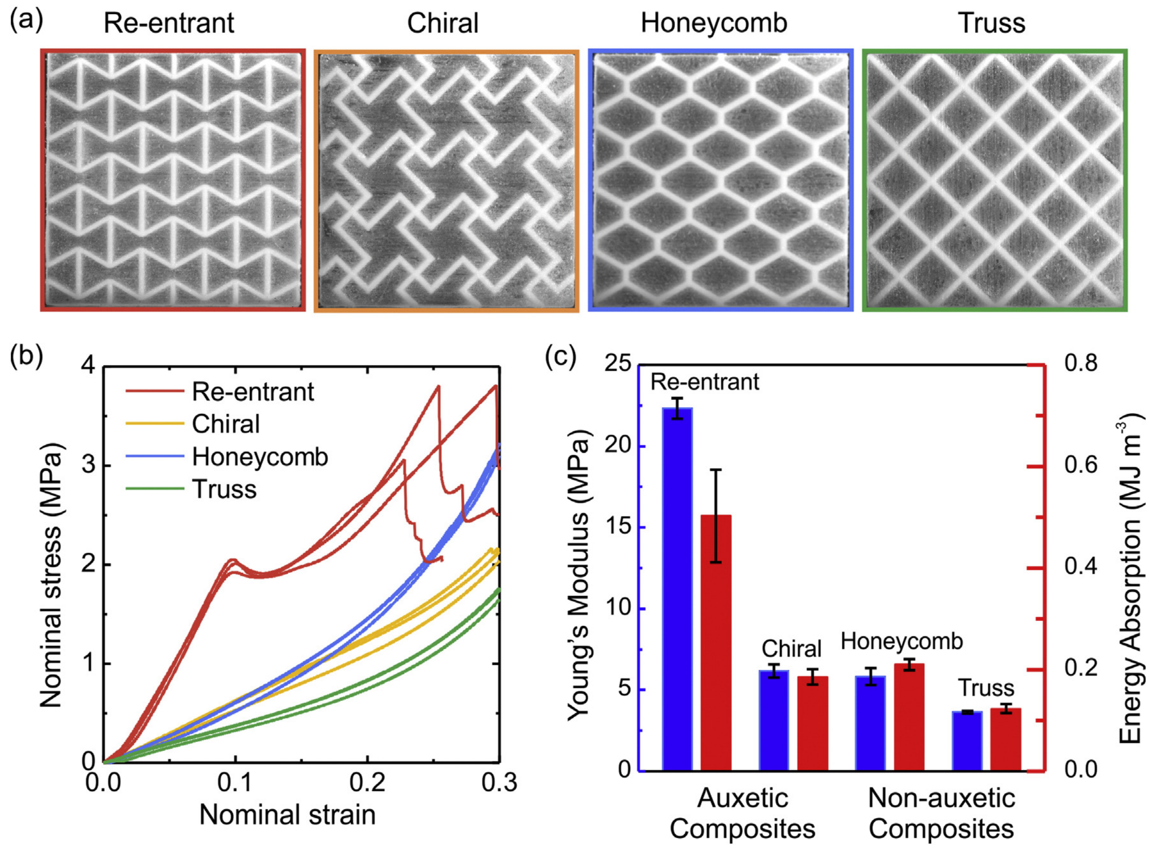

Fig. 3. Mechanical response of the 3D-printed lattice reinforced composites during uniaxial compression tests. (a) The 3D-printed composites with a re-entrant honeycomb reinforced, chiral truss reinforced, regular honeycomb reinforced, and truss reinforced designs. (b) Nominal stress and strain curves for various designs. For each design, three specimens are tested to validate the repeatability. (c) Calculated Young's modulus from the initial linear region of the nominal stress-strain curves and computed energy absorption as the work under the nominal stress-strain curve before 25% uniaxial compressive strain for each composite sample.

matrix phase is only compressed in the vertical direction. By contrast, the elastomer matrix phase of the auxetic reinforced composites, especially the re-entrant honeycomb reinforced composite, is squeezed in both vertical and horizontal directions, indicating a state of biaxial compression. Therefore, the auxetic reinforced composite exhibit significantly enhanced mechanical properties during uniaxial compressive deformation.

3.2. Comparisons between auxetic lattice and auxetic lattice reinforced composites

It is known that typical cellular microstructures are used to achieve a negative Poisson's ratio, so that as expected the stiffness is not that high [28,69]. And based on different deformation mechanisms, existing auxetic cellular solids can be roughly classified into two categories: symmetric units with re-entrant angles, and asymmetric units that rotate when deformed. The deformation mechanism for them is mostly rotation induced bending-dominated. However, some cellular structures such as honeycomb, octet, Kagome, etc., have stretching-dominated deformation mechanism, therefore, exhibiting higher effective stiffness. We have shown that by exploiting the negative Poisson's ratio lattices into the composite design, improved mechanical properties such as stiffness and toughness can be achieved. To further show the superiority of the auxetic lattice reinforced composites, we compare the mechanical properties of lattice reinforced composites and their lattice cellular counterparts under uniaxial compression tests (Fig. 6). The stress-strain curves combined with the experimental deformation images of the composites and their counterpart cellular structures at the compressive strain of 0.25 are also shown in Fig. 6(a)–(d). For the re-entrant honeycomb and chiral cellular structure, the local instability occurs layer by layer with increasing strain, which makes the stress level keep on a plateau. For the regular honeycomb and truss cellular structure, buckling of some local ligaments also makes the stress level on a plateau. By contrast, these composites exhibit a strain hardening effect under the uniaxial compression. This is because the elastomeric matrix phase provides the additional support in these structures, which further increases the stress level. Moreover, combining the lattice phase of glassy polymer with the matrix phase of rubber-like polymer enables the deformation mechanism from the local deformation to the global mechanism. This is because the matrix phase spreads the deformation and decreases both the stress concentration and the local deformation. Therefore, the mutual constraints between two phases of the composites change the local instability to a global instability (auxetic lattices) or local buckling to a global non-catastrophic dissipative event (non-auxetic lattices). The calculated Young's modulus and energy absorption for each composite and its cellular counterpart are presented in Fig. 6(e)–(h). As expected, the typical auxetic cellular structures including re-entrant honeycomb and chiral lattice both exhibit lower stiffness and lower energy absorption comparing to regular honeycomb and truss, as seen in Fig. 6(e) and (g). Because the negative Poisson's ratio of the auxetic cellular structure is obtained through bending and/or rotation inside the microstructure, this also reduces their stiffness as compared to the case of non-auxetic cellular structure with stretching-dominated ligaments. Interestingly, when we use the auxetic lattice structure as a reinforcement phase in a composite, the auxetic behavior will enforce both the stiffness and energy absorption of the composites. For re-entrant honeycomb reinforced composites, the enhancements of stiffness and energy absorption are 9 and 18 times larger than that of the re-entrant honeycomb cellular structures, respectively. However, little enhancement of stiffness is observed in

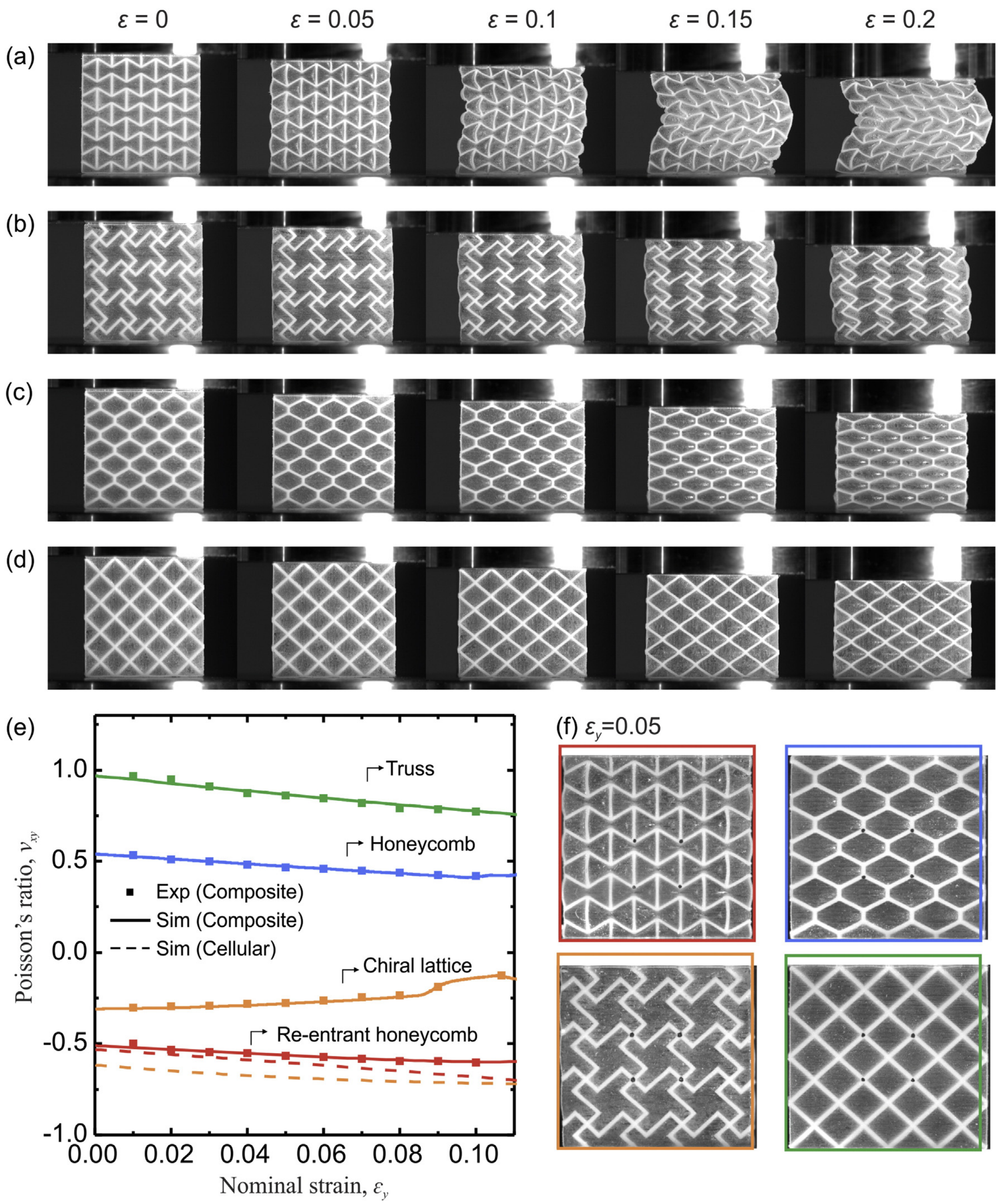

Fig. 4. Experimental images of (a) re-entrant honeycomb reinforced composites, (b) chiral truss reinforced composites, (c) regular honeycomb reinforced composites, and (d) truss reinforced composites at different levels of macroscopic strain: 0, 0.05, 0.1, 0.15 and 0.2 during uniaxial compression tests. (e) Experimental and numerical results of the Poisson's ratios for lattice reinforced composites and the corresponding cellular counterparts under uniaxial compression tests. (f) Experimental images at a macroscopic strain of 0.05 for each composite. The rectangular frames represent the original edges of the specimens before the compressive deformation.

the non-auxetic reinforced composites comparing to their cellular counterparts (see Fig. 6(f)).

To further understand this, finite element simulations are performed on the four types of lattice reinforced composites and the corresponding lattice cellular structures, as shown in Fig. 7. It is clearly noticed that the elastomer phase in the auxetic reinforced composites contributes more significantly to the stress response (and hence enhance the stiffness) than that of the non-auxetic reinforced composites (Fig. 7(a)). The stress level in the elastomer phase in the non-auxetic reinforced composites is much lower, indicating the little contribution of the matrix phase in the load resistance. However, in auxetic reinforced composites, elastomer phase can suppress the bending and rotation of the glassy polymer ligaments, making them more difficult to deform. Furthermore, when comparing the stress contour of lattice structures in the composites and the cellular structures, we clearly find the difference between the auxetic structures and the non-auxetic structures (see Fig. 7 (b) and (c)). In auxetic composites, the ligaments exhibit larger stress comparing with those in auxetic cellular structures, indicating the contribution of them to resist compression loading. In non-auxetic composites, the ligaments show almost the same stress level as those in their

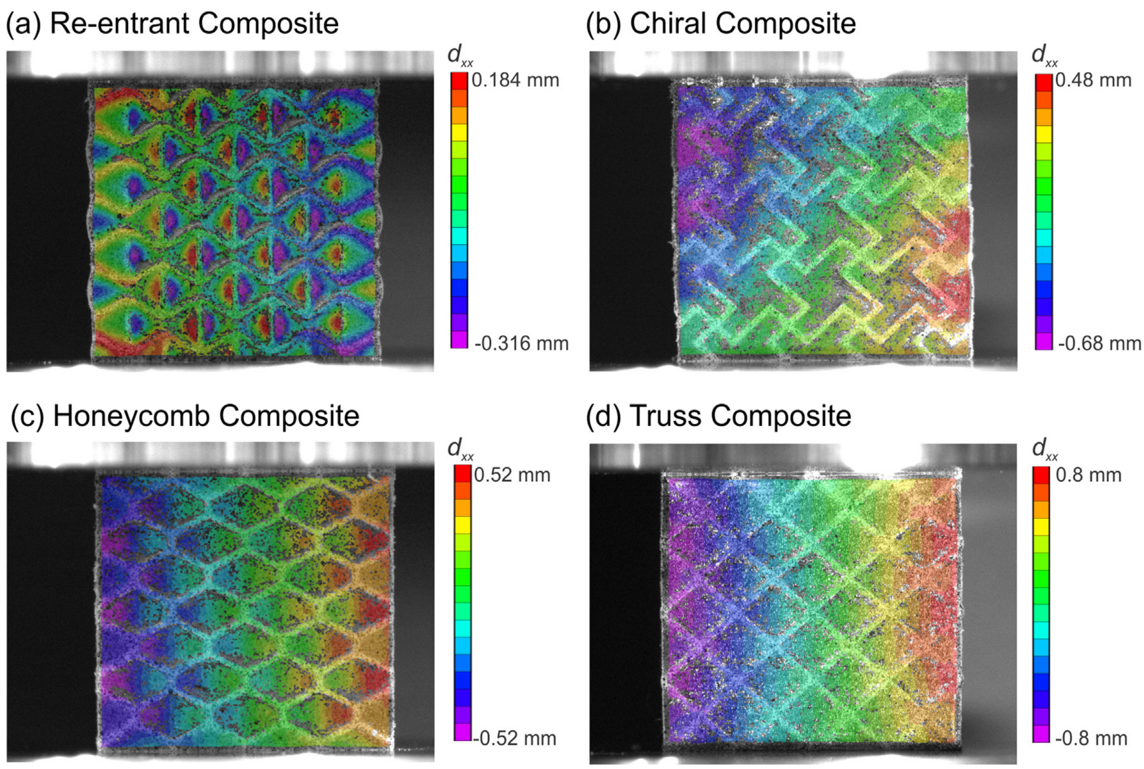

Fig. 5. Experimental displacement contours of (a) the re-entrant honeycomb reinforced composites, (b) the chiral truss reinforced composites, (c) the regular honeycomb reinforced composites, and (d) the truss reinforced composites using digital image correlation at a macroscopic strain of 0.05 during uniaxial compression tests.

counterpart cellular structures, indicating the deformation mechanism for non-auxetic lattice is almost the same both in the composites and cellular structures. Therefore, the mutual constraints between two phases of the auxetic lattice reinforced composites enable enhanced stress resistance by additional support of the matrix phase to the lattice phase. These results suggest the possibility to tailor the auxetic lattices as the reinforcement phase in a composite to achieve enhanced mechanical properties.

3.3. Effect of negative Poisson's ratio

We have demonstrated that the auxetic lattice reinforced composites exhibit enhanced mechanical properties such as stiffness and energy absorption capability compared with non-auxetic lattice reinforced composites. These improved mechanical properties are attributed to the rational structural design of the lattice reinforcement combined with the material selections for the reinforcements and

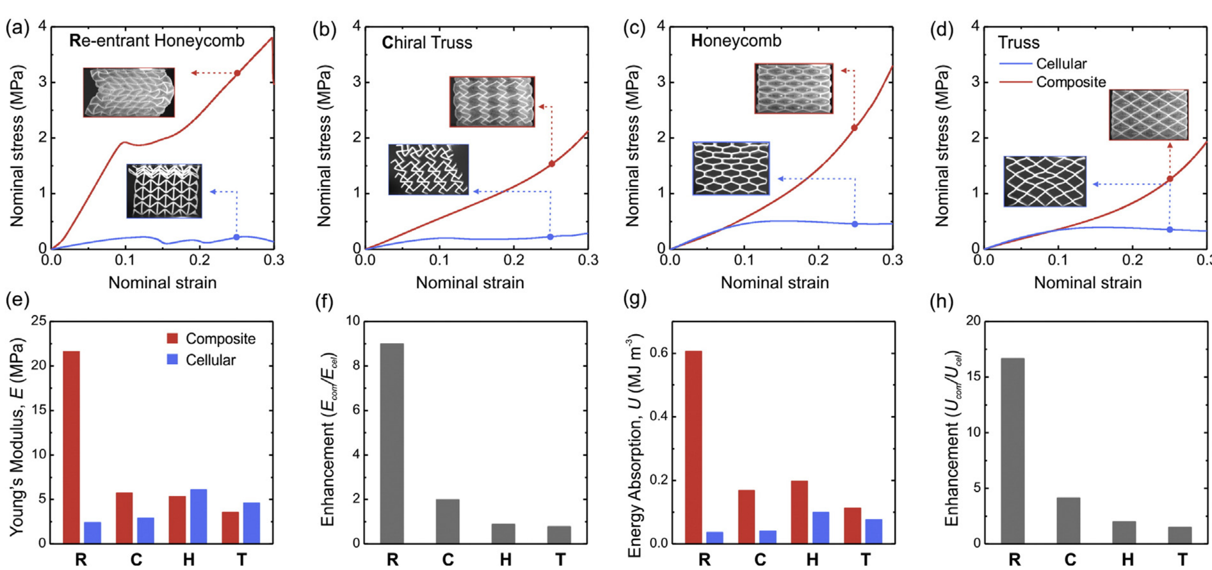

Fig. 6. The comparison of mechanical properties for the lattice reinforced composites and the lattice counterpart structures are shown. The uniaxial compressive stress-strain curves for (a) the re-entrant honeycomb, (b) the chiral truss, (c) the regular honeycomb and (d) the truss lattices for reinforced composites and the corresponding cellular structures, respectively. For each structure, the deformation images of the composite and its counterpart cellular structure at the compressive strain of 0.25 are shown. (e) Calculated Young's modulus and (g) the estimated energy absorption for each specimen. The relative enhancement of (f) Young's modulus and (h) energy absorption of the reinforced composites to their cellular lattice counterparts.

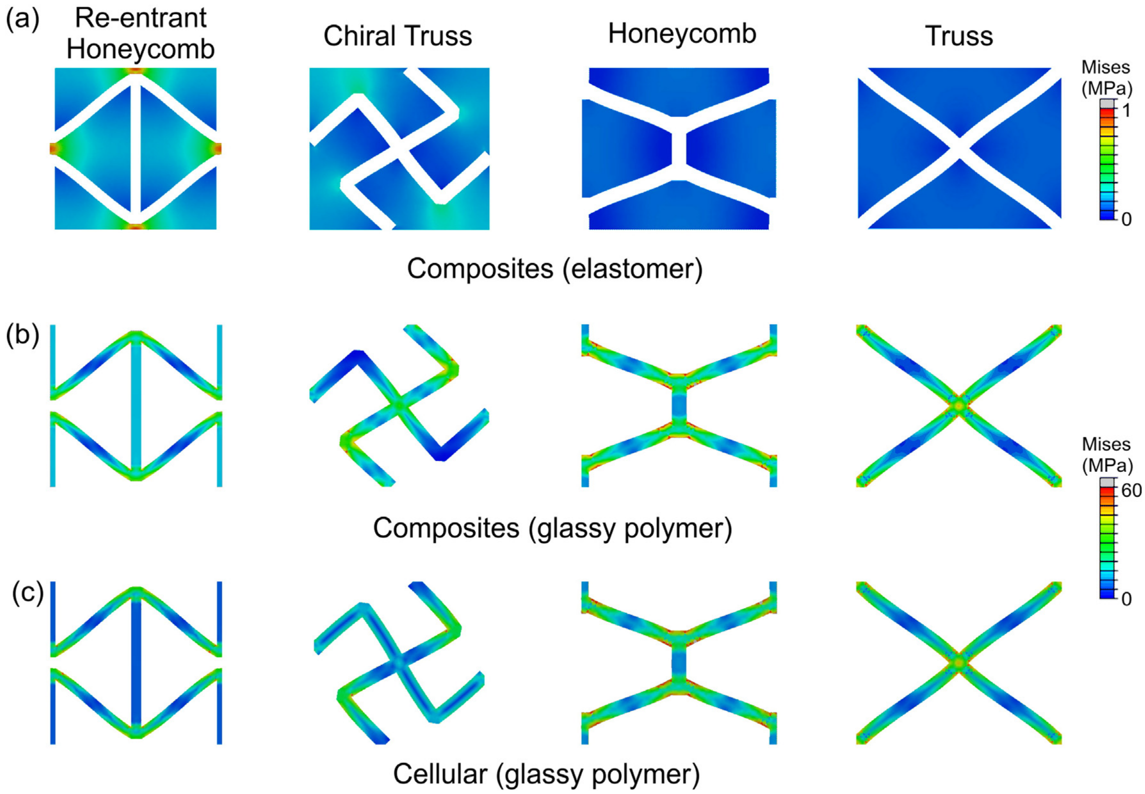

Fig. 7. The von Mises stress distribution in the lattice reinforced composites and the corresponding cellular structures at a nominal compressive strain of 0.05. (a) The von Mises stress distribution in elastomer phase and (b) the reinforcing phase of glassy polymer in reinforced composites. (c) The von Mises stress distribution in the cellular counterparts of a glassy polymer.

matrix phases. In particular, the negative Poisson's ratio in the auxetic reinforcements is crucial to the unusual combination of mechanical performance. To quantitatively understand the effect of Poisson's ratio on the other mechanical properties such as the stiffness and toughness of the lattice reinforced composites, we experimentally explore the response upon compressive tests of the composites reinforced by honeycombs with different Poisson's ratios achieved by varying lattice structure designs. Here we use the same unit cell size as $h = l = 10$ mm, as shown in Fig. 8(a). By assuming the value of Poisson's ratio of each cellular structure as v_{yx}, we calculate that $\theta = \arctan(\nu_{yx} l/h)$, $H = (h - l\tan\theta)/2$ and $L = l/2\cos\theta$, based on Gibson's model [68,70]. Here, the volume fraction of honeycomb reinforcement phase is 20% for each design for a fair comparison. The results reported in Fig. 8(b) indicate that the enhanced mechanical properties are achieved in the presence of the honeycomb designs with the negative Poisson's ratios. Fig. 8(c) shows the corresponding design of honeycomb reinforced composites with Poisson's ratio from −0.9 to 1. Note that when the Poisson's ratio of the composites is zero or positive, the nominal stress-strain curves show a rubber-like hyperelastic behavior; when the Poisson's ratio of the composites is negative, a peak force is observed in the nominal stress-strain curves because the instability occurs in the composites with negative Poisson's ratios. Moreover, the calculated Young's modulus for each composite shows that the honeycomb reinforced composites with lower Poisson's ratios exhibit higher Young's modulus, as shown in Fig. 8(d). For example, the Young's modulus of the composite with a Poisson's ratio of −0.9 is 10 times larger than that of the composite with a Poisson's ratio of 1. Furthermore, the energy absorption at a strain of 0.25 for each composite shows that the honeycomb reinforced composites with negative Poisson's ratios have better energy absorption than the honeycomb reinforced composites with positive Poisson's ratios (Fig. 8(e)). Differently, the composite with a Poisson's ratio of −0.2 exhibits the largest energy absorption capability. This is because the composites with Poisson's ratios smaller than −0.2 have instabilities in earlier strain region and it results in smaller peak stress, leading to lower energy absorption capability. Finally, it is clear that the composites with auxetic reinforcement phase exhibit enhanced mechanical properties comparing to the composites with non-auxetic reinforcement phase. These results offer a complete picture of the effect of Poisson's ratio on the mechanical response of the lattice reinforced composites.

3.4. Effect of volume fraction

While the results reported in Figs. 3–8 are all for composites with the volume fraction of the reinforcement phase as 20%, further tunability can be achieved by altering the volume fraction of the reinforcement phase. Fig. 9 presents the experimental results on the stress-strain response of the four lattice reinforced composites at five different volume fractions from 10% to 50%. The stress-strain curves show an increase in the overall mechanical properties as the volume fraction increases. The results indicate that the auxetic reinforced composites, including the re-entrant honeycomb and the chiral lattice reinforced composites, show clear higher stress level over the non-auxetic reinforced composites from low to high volume fraction of the reinforcement phase. Moreover, when the volume fraction of the reinforcement phase is increased, all the stress-strain curves have a transition from a rubber-like hyperelastic behavior to a highly nonlinear behavior followed by brittle fracture of the reinforced composites. This is because the slenderness ratio of ligaments increases with the increase of the volume fraction of the reinforcement phase, making the reinforcement lattices more brittle. Therefore, continuous loading leads to the local catastrophic failure, resulting in a dramatic drop in the stress-strain curves.

The Young's modulus and energy absorption at a strain of 0.25 calculated from the stress-strain responses are plotted versus the volume fraction of the reinforcement phase in Fig. 10. The re-entrant honeycomb reinforced composite has the highest Young's modulus and

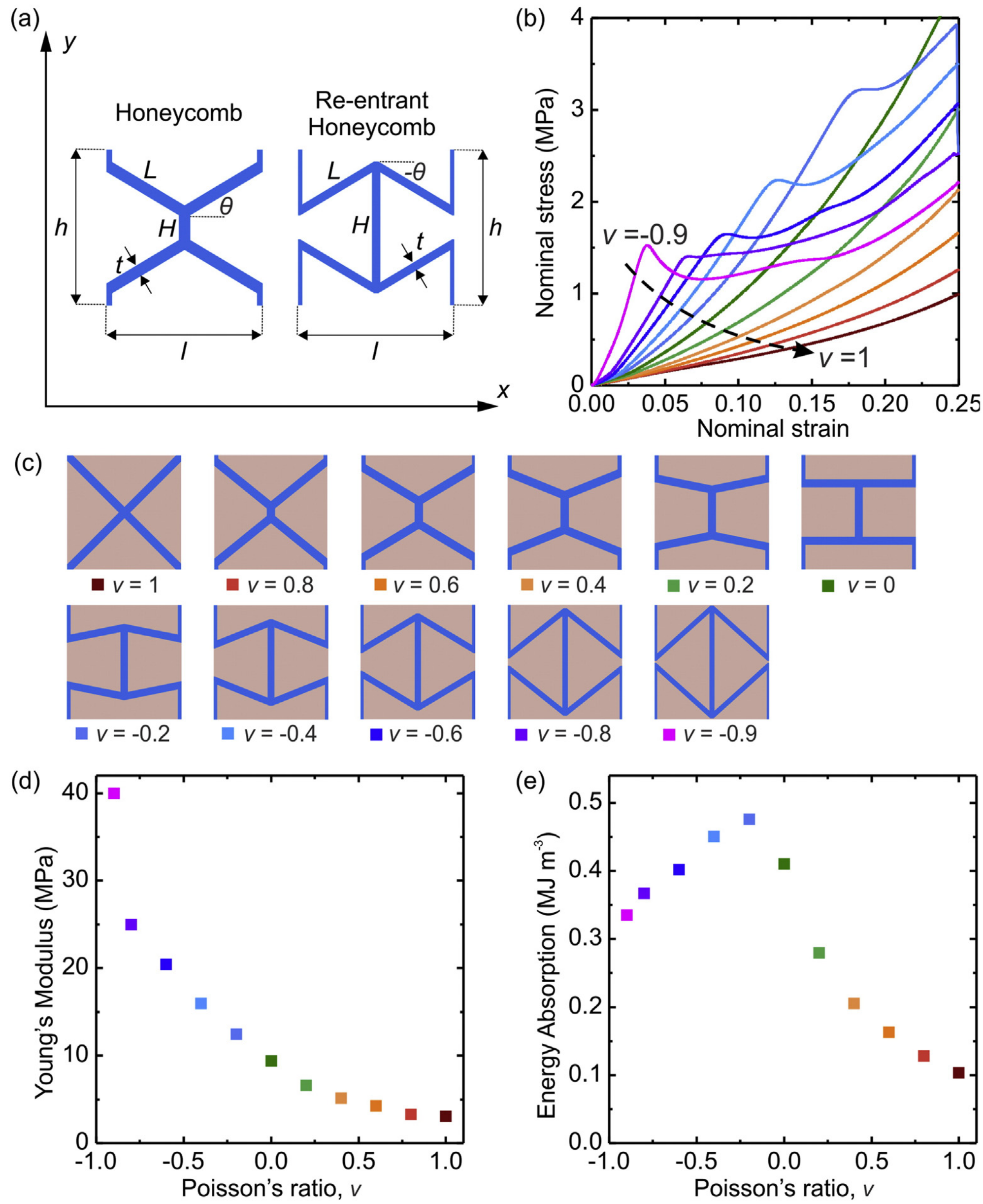

Fig. 8. Effect of Poisson's ratio on the mechanical properties of various honeycomb reinforced composites during the uniaxial compression test. (a) The unit cell geometry and the coordinate system used for regular honeycomb and re-entrant honeycomb. Here, h and l are the unit cell lengths; H is the length of the vertical cell wall and L is the length of the inclined cell wall; t is the thickness of the cell walls; θ is the angle and for re-entrant honeycomb, the value is negative. (b) The nominal stress-strain curves. (c) The geometry design for honeycomb reinforced composites with different Poisson's ratio of the reinforcement honeycombs. (d) Calculated Young's modulus and (e) the estimated energy absorption as a function of the Poisson's ratio of the reinforcement honeycombs.

energy absorption capability comparing to the other three composites, especially at low volume fraction (below 40%) of the reinforcement phase. The chiral lattice reinforced composite is the second best performing composites in general for overall mechanical properties. The non-auxetic lattice reinforced composites exhibit relative weak mechanical properties comparing to auxetic lattice reinforced composites. Generally, the Young's modulus of the cellular materials, such as metal foams and lattice structures, can be described by a scaling law between the mechanical property and the relative density [70,71]. Since the mechanical property of lattice reinforced composites is dominated by the reinforcement phase, we use a scaling law to describe the response of these composites in this study. For the Young's modulus, E_c of the composite can be described as a function of the modulus of material for reinforcement phase, E_r and the volume fraction of the reinforcement phase, V_r/V_c, via $E_c = C_1E_r(V_r/V_c)^n$ where C_1 and n can be obtained by fitting the experimental data. Similar relation for energy absorption, U_c is $U_c = C_2U_r(V_r/V_c)^m$ where U_r is the energy absorption of the bulk material of the reinforcement phase at the same strain level, presented in Table 1; C_2 and m can be obtained by fitting the experimental data. The parameters C_1, C_2, n and m are listed in Table 2. The scaling exponent close to 1 indicates a stretch-dominated deformation behavior whereas an exponent of 2 typically indicates bending-dominated deformation. It is also established that structures governed by a stretching-dominated deformation offer higher stiffness and strength per unit weight than those governed by bending-dominated deformation. In our lattice reinforced composites, the scaling exponent for re-entrant honeycomb reinforced composites are found to be $n = 1.369$ and $m = 1.174$. While for the other composites, the scaling exponents are larger or close to 2. These results indicate that the re-entrant honeycomb reinforced composites are close to stretch-dominated deformation in overall while the other composites are close to bending-dominated during uniaxial compressive loading. Moreover, this trend

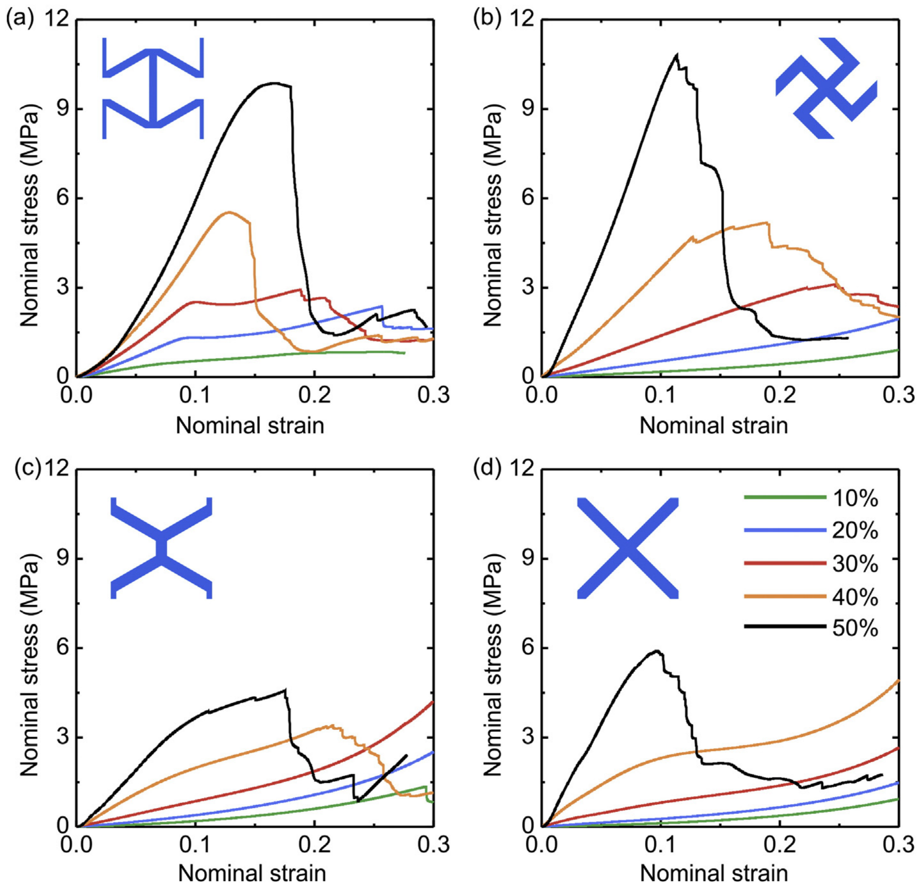

Fig. 9. The stress-strain responses of four types of composites at different volume fractions of the reinforcing phase. (a) Re-entrant honeycomb reinforced composites, (b) chiral truss reinforced composites, (c) regular honeycomb reinforced composites, and (d) truss reinforced composites.

can be noticed in the local analyses of the composites (Fig. 7). Notice that in the honeycomb and the truss composites, the matrix has neglectable effects on the deformation mechanism of the lattice structures. We believe that the deformation mechanisms of non-auxetic composites and cellular structures are more bending-dominated. However, in the re-entrant and the chiral truss composites, the matrix provides additional support and suppresses the bending and rotation of the ligaments of the lattice structures, making them more difficult to deform, changing the deformation mechanism to more stretching-dominated. As a result, the deformation mechanism significantly affects the mechanical response of the lattice reinforced composites. This nearly linear scaling relation of the re-entrant honeycomb reinforced composites indicates that we can design light weight yet stronger composites. These results suggest great potentials to tailor the geometric features of the lattice reinforced composites to achieve tunable mechanical properties.

4. Discussions

In the previous sections, we focus on the 2D lattice structures and demonstrate that 2D auxetic lattice reinforced composites exhibit enhanced mechanical properties. Recently, 3D auxetic systems consisting of networks of buckliball [72], chiral-like structures [73], orthotropic laminated open-cell frameworks [74], and lattice metamaterials with curved beams [75–77] have been designed. Indeed, most of these 3D auxetic structures are porous thus are very suitable to serve as reinforcements in composites. Conceptually, under uniaxial compression, the soft matrix will be in a state of triaxial compression, thereby leveraging the overall mechanical performance of the composites [78–80].

In this study, we focus on demonstrating the effect of geometric features of auxetic reinforcements on the mechanical behaviors of the designed composites, however, the selection of materials for each phase of composites is still an important issue. Due to the limitation of our 3D printer, we use the glassy polymer as the reinforcement phase and a rubber-like material as the matrix. Recently, additive manufacturing enables the fabrication of not only polymeric but also metallic and ceramic materials with intricate cellular architectures [62]. Cellular materials, such as lattice structures, can easily be fabricated by metal powder bed fusion [81,82]. Although given the high melting point of ceramics, a few 3D printing systems could print ceramics either by selective curing of a photosensitive resin that contains ceramic particles, by binder jetting or by selective fusion of a powder bed with a laser [83,84]. Moreover, post-pyrolysis of 3D printed polymer precursors can fabricate carbon [85,86] or ceramic materials [87] with architected structures. Therefore, as new methods are emerging and maturing, fabrication of more and more complex cellular architectures especially auxetic structures will be enabled. Such development will facilitate fabricating auxetic reinforced composites with various materials as the reinforcement phase for a wide range of applications and further creating multifunctional materials.

Finally, the dynamic response of the auxetic reinforced composites will be of great interest despite we have studied the quasi-static compressive behaviors here. For example, improved impact resistance has been recently observed in 3D-printed bioinspired composites with hierarchical conch shell structures using the same material systems as ours [88]. Indeed, the dynamic effects including the micro-inertial effect, shock wave effect, and strain rate effect of the materials have significant influences to the mechanical behaviors of the 3D-printed composites. For instance, the yield strength of the glassy polymer VeroWhite clearly increases as the strain rate increases. In the future work, the dynamic behaviors of the auxetic reinforced composites under different levels of strain rates will be systematically investigated.

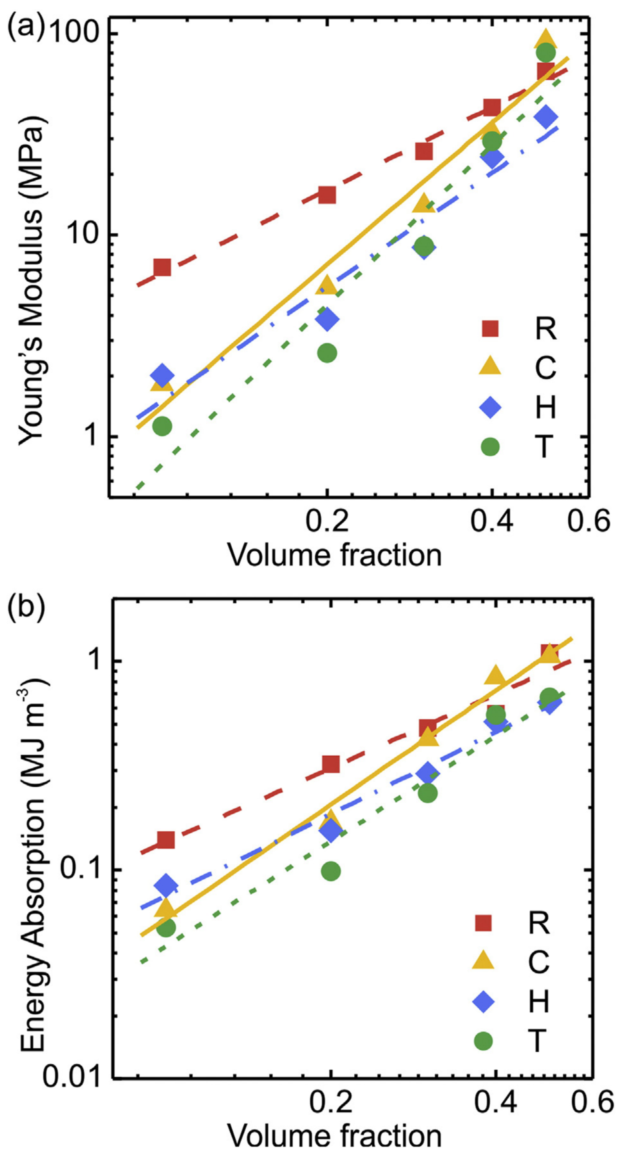

Fig. 10. Comparison of mechanical properties of the lattice reinforced composites as a function of the volume fraction of reinforcement phase: (a) Young's modulus, (b) energy absorption.

5. Conclusions

In summary, we have investigated the macroscopic mechanical responses of the auxetic lattice reinforced composites through a combination of 3D printing, experiments, and numerical analyses. We have shown that auxetic lattice reinforced composites have enhanced mechanical performance, achieving a unique combination of stiffness and energy absorption, compared with the non-auxetic lattice reinforced composites. In particular, by harnessing the negative Poisson's ratio effect in the lattice reinforcements, we find that the mutual constraints between the auxetic reinforcement and matrix enable enhanced mechanical properties by gaining additional support from the matrix phase. We further quantify the effect of Poisson's ratio on the other mechanical properties of various honeycomb reinforced composites, indicating that the degree of auxetic behavior could be used to tune the stiffness and energy absorption of the lattice reinforced composites. Finally, we use scaling law to evaluate the effect of volume fraction of the reinforcement phase in the composites, showing that the re-entrant honeycomb reinforced composite exhibit nearly linear scaling. These results provide guidelines for engineering and developing a new class of auxetic reinforced composites with enhanced mechanical performance for a wide range of applications and further creating multifunctional materials.

Table 2
The relations of the Young's modulus and energy absorption at a strain of 0.25 to the volume fraction of the reinforcement phase for the lattice reinforced composites.

Lattice reinforced composites	Young's modulus		Energy absorption	
	C_1	n	C_2	m
Re-entrant composite	0.100	1.369	0.186	1.174
Chiral composite	0.204	2.340	0.349	1.817
Honeycomb composite	0.075	1.877	0.138	1.303
Truss composite	0.206	2.630	0.186	1.676

Acknowledgements

The authors gratefully acknowledge the financial support from the National Science Foundation (CMMI-1437449, CMMI-1462270), and the Office of Naval Research (Dr. Yapa Rajapakse, Solid Mechanics Program).

References

[1] K.E. Evans, Auxetic polymers: a new range of materials, Endeavour 15 (4) (1991) 170–174.
[2] R.H. Baughman, J.M. Shacklette, A.A. Zakhidov, S. Stafstrom, Negative Poisson's ratios as a common feature of cubic metals, Nature 392 (6674) (1998) 362.
[3] J.N. Grima, R. Jackson, A. Alderson, K.E. Evans, Do zeolites have negative Poisson's ratios? Adv. Mater. 12 (24) (2000) 1912–1918.
[4] J.N. Grima, R. Gatt, V. Zammit, J.J. Williams, K.E. Evans, A. Alderson, R.I. Walton, Natrolite: a zeolite with negative Poisson's ratios, J. Appl. Phys. 101 (8) (2007), 086102.
[5] F. Song, J. Zhou, X. Xu, Y. Xu, Y. Bai, Effect of a negative Poisson ratio in the tension of ceramics, Phys. Rev. Lett. 100 (24) (2008), 245502. .
[6] A. Yeganeh-Haeri, D.J. Weidner, J.B. Parise, Elasticity of or-cristobalitez A silicon dioxide with a negative Poisson's ratio, Science 257 (1992) 31.
[7] J.-W. Jiang, H.S. Park, Negative poisson's ratio in single-layer graphene ribbons, Nano Lett. 16 (4) (2016) 2657–2662.
[8] J.N. Grima, S. Winczewski, L. Mizzi, M.C. Grech, R. Cauchi, R. Gatt, D. Attard, K.W. Wojciechowski, J. Rybicki, Tailoring graphene to achieve negative Poisson's ratio properties, Adv. Mater. 27 (8) (2015) 1455–1459.
[9] Y. Suzuki, G. Cardone, D. Restrepo, P.D. Zavattieri, T.S. Baker, F.A. Tezcan, Self-assembly of coherently dynamic, auxetic two-dimensional protein crystals, Nature 533 (7603) (2016) 369.
[10] R. Lakes, Foam structures with a negative Poisson's ratio, Science 235 (1987) 1038–1041.
[11] R. Lakes, K. Elms, Indentability of conventional and negative Poisson's ratio foams, J. Compos. Mater. 27 (12) (1993) 1193–1202.
[12] W. Yang, Z.-M. Li, W. Shi, B.-H. Xie, M.-B. Yang, Review on auxetic materials, J. Mater. Sci. 39 (10) (2004) 3269–3279.
[13] J.N. Grima, K.E. Evans, Auxetic behavior from rotating squares, J. Mater. Sci. Lett. 19 (17) (2000) 1563–1565.
[14] J. Choi, R. Lakes, Fracture toughness of re-entrant foam materials with a negative Poisson's ratio: experiment and analysis, Int. J. Fract. 80 (1) (1996) 73–83.
[15] A. Alderson, K. Alderson, Auxetic materials, Proc. IME G J. Aerosp. Eng. 221 (4) (2007) 565–575.
[16] S. Mohsenizadeh, R. Alipour, M.S. Rad, A.F. Nejad, Z. Ahmad, Crashworthiness assessment of auxetic foam-filled tube under quasi-static axial loading, Mater. Des. 88 (2015) 258–268.
[17] S. Hou, T. Liu, Z. Zhang, X. Han, Q. Li, How does negative Poisson's ratio of foam filler affect crashworthiness? Mater. Des. 82 (2015) 247–259.
[18] T. Li, L. Wang, Bending behavior of sandwich composite structures with tunable 3D-printed core materials, Compos. Struct. 175 (2017) 46–57.
[19] L.F. Wang, M.C. Boyce, Bioinspired structural material exhibiting post-yield lateral expansion and volumetric energy dissipation during tension, Adv. Funct. Mater. 20 (18) (2010) 3025–3030.
[20] Z. Wang, H. Hu, Auxetic materials and their potential applications in textiles, Text. Res. J. 84 (15) (2014) 1600–1611.
[21] Z. Ge, H. Hu, Innovative three-dimensional fabric structure with negative Poisson's ratio for composite reinforcement, Text. Res. J. 83 (5) (2013) 543–550.
[22] Y. Liu, H. Hu, J.K. Lam, S. Liu, Negative Poisson's ratio weft-knitted fabrics, Text. Res. J. 80 (9) (2010) 856–863.
[23] H. Hu, Z. Wang, S. Liu, Development of auxetic fabrics using flat knitting technology, Text. Res. J. 81 (14) (2011) 1493–1502.
[24] Z.-D. Ma, H. Bian, C. Sun, G.M. Hulbert, K. Bishnoi, F. Rostam-Abadi, Functionally-graded NPR (Negative Poisson's Ratio) Material for a Blast-protective Deflector, Michigan Univ, Ann Arbor, 2010.
[25] G. Stavroulakis, Auxetic behaviour: appearance and engineering applications, Phys. Status Solidi B 242 (3) (2005) 710–720.

[26] Z.-D. Ma, Y. Liu, X. Liu, C. Sun, Y. Cui, Ultralightweight runflat tires based upon negative Poisson ratio (NPR) auxetic structures, Google Patents, 2013.
[27] F. Scarpa, Auxetic materials for bioprostheses [in the spotlight], IEEE Signal Process. Mag. 25 (5) (2008) 128–126.
[28] Y. Liu, H. Hu, A review on auxetic structures and polymeric materials, Sci. Res. Essays 5 (10) (2010) 1052–1063.
[29] Q. Liu, Literature Review: Materials With Negative Poisson's Ratios and Potential Applications to Aerospace and Defence, Defence Science and Technology Organisation Victoria (Australia) Air Vehicles Div, 2006.
[30] K.W. Wojciechowski, Constant thermodynamic tension Monte Carlo studies of elastic properties of a two-dimensional system of hard cyclic hexamers, Mol. Phys. 61 (5) (1987) 1247–1258.
[31] A.A. Pozniak, J. Smardzewski, K.W. Wojciechowski, Computer simulations of auxetic foams in two dimensions, Smart Mater. Struct. 22 (8) (2013), 084009. .
[32] L.J. Gibson, M. Ashby, G. Schajer, C. Robertson, The mechanics of two-dimensional cellular materials, Proceedings of the Royal Society of London A: Mathematical, Physical and Engineering Sciences, The Royal Society 1982, pp. 25–42.
[33] A. Kolpakov, On the determination of the averaged moduli of elastic gridworks, Prikl. Mat. Mekh 59 (1985) 969–977.
[34] K. El Nady, F. Dos Reis, J.F. Ganghoffer, Computation of the homogenized nonlinear elastic response of 2D and 3D auxetic structures based on micropolar continuum models, Compos. Struct. 170 (Supplement C) (2017) 271–290.
[35] D. Prall, R. Lakes, Properties of a chiral honeycomb with a Poisson's ratio of—1, Int. J. Mech. Sci. 39 (3) (1997) 305–314.
[36] C.W. Smith, J. Grima, K. Evans, A novel mechanism for generating auxetic behaviour in reticulated foams: missing rib foam model, Acta Mater. 48 (17) (2000) 4349–4356.
[37] Y. Jiang, Y. Li, 3D printed chiral cellular solids with amplified auxetic effects due to elevated internal rotation, Adv. Eng. Mater. 19 (2) (2017).
[38] P. Vogiatzis, S. Chen, X. Wang, T. Li, L. Wang, Topology optimization of multi-material negative Poisson's ratio metamaterials using a reconciled level set method, Comput. Aided Des. 83 (2017) 15–32.
[39] K. ElNady, I. Goda, J.-F. Ganghoffer, Computation of the effective nonlinear mechanical response of lattice materials considering geometrical nonlinearities, Comput. Mech. 58 (6) (2016) 957–979.
[40] N. Karathanasopoulos, H. Reda, J.-f. Ganghoffer, Designing two-dimensional metamaterials of controlled static and dynamic properties, Comput. Mater. Sci. 138 (Supplement C) (2017) 323–332.
[41] K. Wojciechowski, Two-dimensional isotropic system with a negative Poisson ratio, Phys. Lett. A 137 (1–2) (1989) 60–64.
[42] A. Pozniak, K. Wojciechowski, Poisson's ratio of rectangular anti-chiral structures with size dispersion of circular nodes, Phys. Status Solidi B 251 (2) (2014) 367–374.
[43] J.N. Grima, A. Alderson, K. Evans, Auxetic behaviour from rotating rigid units, Phys. Status Solidi B 242 (3) (2005) 561–575.
[44] G.W. Milton, Complete characterization of the macroscopic deformations of periodic unimode metamaterials of rigid bars and pivots, J. Mech. Phys. Solids 61 (7) (2013) 1543–1560.
[45] H. Yasuda, J. Yang, Reentrant origami-based metamaterials with negative Poisson's ratio and bistability, Phys. Rev. Lett. 114 (18) (2015), 185502. .
[46] C. Lv, D. Krishnaraju, G. Konjevod, H. Yu, H. Jiang, Origami based mechanical metamaterials, Sci. Rep. 4 (2014).
[47] Y. Hou, R. Neville, F. Scarpa, C. Remillat, B. Gu, M. Ruzzene, Graded conventional-auxetic Kirigami sandwich structures: flatwise compression and edgewise loading, Compos. Part B 59 (2014) 33–42.
[48] S. Shan, S.H. Kang, Z. Zhao, L. Fang, K. Bertoldi, Design of planar isotropic negative Poisson's ratio structures, Extreme Mech. Lett. 4 (2015) 96–102.
[49] Y. Tang, J. Yin, Design of cut unit geometry in hierarchical kirigami-based auxetic metamaterials for high stretchability and compressibility, Extreme Mech. Lett. 12 (2017) 77–85.
[50] G. Wu, Y. Cho, I.S. Choi, D. Ge, J. Li, H.N. Han, T. Lubensky, S. Yang, Directing the deformation paths of soft metamaterials with prescribed asymmetric units, Adv. Mater. 27 (17) (2015) 2747–2752.
[51] Y. Cho, J.-H. Shin, A. Costa, T.A. Kim, V. Kunin, J. Li, S.Y. Lee, S. Yang, H.N. Han, I.-S. Choi, Engineering the shape and structure of materials by fractal cut, Proc. Natl. Acad. Sci. 111 (49) (2014) 17390–17395.
[52] Y. Tang, G. Lin, L. Han, S. Qiu, S. Yang, J. Yin, Design of hierarchically cut hinges for highly stretchable and reconfigurable metamaterials with enhanced strength, Adv. Mater. 27 (44) (2015) 7181–7190.
[53] V.V. Novikov, K.W. Wojciechowski, Negative Poisson coefficient of fractal structures, Phys. Solid State 41 (12) (1999) 1970–1975.
[54] P.M. Pigłowski, J.W. Narojczyk, A.A. Poźniak, K.W. Wojciechowski, K.V. Tretiakov, Auxeticity of Yukawa systems with nanolayers in the (111) crystallographic plane, Materials 10 (11) (2017) 1338.
[55] T.C. Lim, Analogies across auxetic models based on deformation mechanism, Phys. Status Solidi RRL 11 (6) (2017), 1600440.
[56] V. Simkins, A. Alderson, P. Davies, K. Alderson, Single fibre pullout tests on auxetic polymeric fibres, J. Mater. Sci. 40 (16) (2005) 4355–4364.
[57] K. Alderson, V. Simkins, V. Coenen, P. Davies, A. Alderson, K. Evans, How to make auxetic fibre reinforced composites, Phys. Status Solidi B 242 (3) (2005) 509–518.
[58] S. Jayanty, J. Crowe, L. Berhan, Auxetic fibre networks and their composites, Phys. Status Solidi B 248 (1) (2011) 73–81.
[59] Z. Ge, H. Hu, Y. Liu, A finite element analysis of a 3D auxetic textile structure for composite reinforcement, Smart Mater. Struct. 22 (8) (2013), 084005. .
[60] L. Zhou, L. Jiang, H. Hu, Auxetic composites made of 3D textile structure and polyurethane foam, Phys. Status Solidi B 253 (7) (2016) 1331–1341.
[61] A.A. Poźniak, K.W. Wojciechowski, J.N. Grima, L. Mizzi, Planar auxeticity from elliptic inclusions, Compos. Part B 94 (Supplement C) (2016) 379–388.
[62] T.A. Schaedler, W.B. Carter, Architected cellular materials, Annu. Rev. Mater. Res. 46 (2016) 187–210.
[63] X. Wang, M. Jiang, Z. Zhou, J. Gou, D. Hui, 3D printing of polymer matrix composites: a review and prospective, Compos. Part B 110 (2017) 442–458.
[64] T. Fíla, P. Zlámal, O. Jiroušek, J. Falta, P. Koudelka, D. Kytýř, T. Doktor, J. Valach, Impact testing of polymer-filled auxetics using split Hopkinson pressure bar, Adv. Eng. Mater. 19 (10) (2017), 1700076.
[65] R. Zhang, H.-L. Yeh, H.-Y. Yeh, A preliminary study of negative Poisson's ratio of laminated fiber reinforced composites, J. Reinf. Plast. Compos. 17 (18) (1998) 1651–1664.
[66] P. Zhang, A.C. To, Transversely isotropic hyperelastic-viscoplastic model for glassy polymers with application to additive manufactured photopolymers, Int. J. Plast. 80 (Supplement C) (2016) 56–74.
[67] E.M. Arruda, M.C. Boyce, A three-dimensional constitutive model for the large stretch behavior of rubber elastic materials, J. Mech. Phys. Solids 41 (2) (1993) 389–412.
[68] I. Masters, K. Evans, Models for the elastic deformation of honeycombs, Compos. Struct. 35 (4) (1996) 403–422.
[69] H.M.A. Kolken, A.A. Zadpoor, Auxetic mechanical metamaterials, RSC Adv. 7 (9) (2017) 5111–5129.
[70] L.J. Gibson, M.F. Ashby, Cellular Solids: Structure and Properties, Cambridge University Press, 1999.
[71] M. Ashby, The properties of foams and lattices, Philos. Trans. R. Soc. Lond. A Math. Phys. Eng. Sci. 364 (1838) (2006) 15–30.
[72] S. Babaee, J. Shim, J.C. Weaver, E.R. Chen, N. Patel, K. Bertoldi, 3D soft metamaterials with negative Poisson's ratio, Adv. Mater. 25 (36) (2013) 5044–5049.
[73] C.S. Ha, M.E. Plesha, R.S. Lakes, Chiral three-dimensional lattices with tunable Poisson's ratio, Smart Mater. Struct. 25 (5) (2016), 054005. .
[74] H. Tanaka, K. Suga, N. Iwata, Y. Shibutani, Orthotropic laminated open-cell frameworks retaining strong auxeticity under large uniaxial loading, Sci. Rep. 7 (2017), 39816. .
[75] Y. Chen, T. Li, F. Scarpa, L. Wang, Lattice metamaterials with mechanically tunable Poisson's ratio for vibration control, Phys. Rev. Appl. 7 (2) (2017), 024012. .
[76] F. Warmuth, F. Osmanlic, L. Adler, M.A. Lodes, C. Körner, Fabrication and characterisation of a fully auxetic 3D lattice structure via selective electron beam melting, Smart Mater. Struct. 26 (2) (2016), 025013. .
[77] T. Li, X. Hu, Y. Chen, L. Wang, Harnessing out-of-plane deformation to design 3D architected lattice metamaterials with tunable Poisson's ratio, Sci. Rep. 7 (1) (2017) 8949.
[78] L. Wang, J. Lau, E.L. Thomas, M.C. Boyce, Co-continuous composite materials for stiffness, strength, and energy dissipation, Adv. Mater. 23 (13) (2011) 1524–1529.
[79] J.-H. Lee, L. Wang, S. Kooi, M.C. Boyce, E.L. Thomas, Enhanced energy dissipation in periodic epoxy nanoframes, Nano Lett. 10 (7) (2010) 2592–2597.
[80] Y.L. Liu, L.F. Wang, Enhanced stiffness, strength and energy absorption for co-continuous composites with liquid filler, Compos. Struct. 128 (2015) 274–283.
[81] T.J. Horn, O.L. Harrysson, Overview of current additive manufacturing technologies and selected applications, Sci. Prog. 95 (3) (2012) 255–282.
[82] O. Cansizoglu, O. Harrysson, D. Cormier, H. West, T. Mahale, Properties of Ti–6Al–4V non-stochastic lattice structures fabricated via electron beam melting, Mater. Sci. Eng. A 492 (1) (2008) 468–474.
[83] K. Leuven, Additive manufacturing of ceramics: a review, J. Ceram. Sci. Technol. 5 (4) (2014) 245–260.
[84] A. Zocca, P. Colombo, C.M. Gomes, J. Günster, Additive manufacturing of ceramics: issues, potentialities, and opportunities, J. Am. Ceram. Soc. 98 (7) (2015) 1983–2001.
[85] A. Szczurek, A. Ortona, L. Ferrari, E. Rezaei, G. Medjahdi, V. Fierro, D. Bychanok, P. Kuzhir, A. Celzard, Carbon periodic cellular architectures, Carbon 88 (2015) 70–85.
[86] J.-H. Lee, L. Wang, M.C. Boyce, E.L. Thomas, Periodic bicontinuous composites for high specific energy absorption, Nano Lett. 12 (8) (2012) 4392–4396.
[87] Z.C. Eckel, C. Zhou, J.H. Martin, A.J. Jacobsen, W.B. Carter, T.A. Schaedler, Additive manufacturing of polymer-derived ceramics, Science 351 (6268) (2016) 58–62.
[88] G.X. Gu, M. Takaffoli, M.J. Buehler, Hierarchically enhanced impact resistance of bioinspired composites, Adv. Mater. 29 (28) (2017).